Oncogenic β-catenin and PIK3CA instruct network states and cancer phenotypes in intestinal organoids

Pamela Riemer,[1,2] Mattias Rydenfelt,[3] Matthias Marks,[4] Karen van Eunen,[5] Kathrin Thedieck,[5] Bernhard G. Herrmann,[4] Nils Blüthgen,[1,3] Christine Sers,[1,2] and Markus Morkel[1]

[1]Laboratory of Molecular Tumor Pathology, Institute of Pathology, Charité Universitätsmedizin Berlin, 10117 Berlin, Germany
[2]German Cancer Consortium, German Cancer Research Center, 69120 Heidelberg, Germany
[3]Integrative Research Institute Life Sciences, Humboldt University Berlin, 10099 Berlin, Germany
[4]Department of Developmental Genetics, Max Planck Institute for Molecular Genetics, 14195 Berlin, Germany
[5]Department of Pediatrics, Center for Liver, Digestive and Metabolic Diseases, University Medical Center Groningen, 9713 GZ Groningen, Netherlands

Colorectal cancer is driven by cooperating oncogenic mutations. In this study, we use organotypic cultures derived from transgenic mice inducibly expressing oncogenic β-catenin and/or PIK3CA^{H1047R} to follow sequential changes in cancer-related signaling networks, intestinal cell metabolism, and physiology in a three-dimensional environment mimicking tissue architecture. Activation of β-catenin alone results in the formation of highly clonogenic cells that are nonmotile and prone to undergo apoptosis. In contrast, coexpression of stabilized β-catenin and PIK3CA^{H1047R} gives rise to intestinal cells that are apoptosis-resistant, proliferative, stem cell–like, and motile. Systematic inhibitor treatments of organoids followed by quantitative phenotyping and phosphoprotein analyses uncover key changes in the signaling network topology of intestinal cells after induction of stabilized β-catenin and PIK3CA^{H1047R}. We find that survival and motility of organoid cells are associated with 4EBP1 and AKT phosphorylation, respectively. Our work defines phenotypes, signaling network states, and vulnerabilities of transgenic intestinal organoids as a novel approach to understanding oncogene activities and guiding the development of targeted therapies.

Introduction

Colorectal cancer (CRC) arises by sequential acquisition of mutations in cells of the intestinal epithelium (Fearon, 2011). Until recently, the early steps in this process could not faithfully be analyzed in vitro because CRC cell lines are usually derived from advanced carcinomas. In contrast, organoids can be established from normal tissue and any stage of malignant progression (Sato et al., 2009, 2011b). Thus, organoids are well suited to study oncogene interaction in intestinal cells.

CRC is most frequently initiated by mutations activating the Wnt–β-catenin signaling pathway, such as by loss of the tumor suppressor and β-catenin regulator adenomatous polyposis coli (APC) or by mutations in β-catenin that prevent degradation. These mutations stabilize stem cell fate (Clevers et al., 2014). Functional loss of APC and stabilizing mutations in β-catenin have similar effects in intestinal organoids (Farrall et al., 2012). The phosphatidylinositol-3-kinase (PI3K) signaling cascade is often activated during CRC progression, frequently by hotspot mutations in the catalytic kinase subunit PIK3CA (Parsons et al., 2005; The Cancer Genome Atlas Network, 2012). Oncogenic PIK3CA operates via the kinase AKT, which can directly phosphorylate cytoskeletal targets to regulate cell motility and invasion (Xue and Hemmings, 2013), the mechanistic target of rapamycin (mTOR) complex 1 (mTORC1), which integrates cell signal transduction, translation, and metabolic regulation (Song et al., 2012), and FOXO-type transcription factors (Jacinto et al., 2006; Tzivion and Hay, 2011).

The mouse small intestine is a well-established model system to interrogate signaling networks relevant for human colon cancer. In this study, we used organoids of the mouse small intestine to study cooperation of oncogenic Wnt–β-catenin and PI3K activities. We found that mutant stabilized β-catenin (CTNNB1^{stab}) and PIK3CA^{H1047R} induce multiple hallmark traits of cancer that are not immediately apparent in 2D cell line cultures or in transgenic mouse models. We discovered that the induction of cell attachment and motility via PIK3CA^{H1047R} depends on active β-catenin. By using a panel of pharmaceutical inhibitors in combination with phenotypic assays and phosphoprotein profiling, we link cell survival and motility to 4EBP1 and AKT phosphorylation, respectively.

Correspondence to Markus Morkel: markus.morkel@charite.de

Abbreviations used: APC, adenomatous polyposis coli; CCM, crypt culture medium; CRC, colorectal cancer; EC, enzyme commission; EMT, epithelial–mesenchymal transition; ERK, extracellular signal-related kinase; GSEA, gene set enrichment analysis; MEK, MAPK kinase; mTOR, mechanistic target of rapamycin; NADH, nicotinamide adenine dinucleotide; PI3K, phosphatidylinositol-3-kinase.

The Rockefeller University Press $30.00
J. Cell Biol. Vol. 216 No. 6 1567–1577
https://doi.org/10.1083/jcb.201610058

Results and discussion

The CTNNB1^{stab} and PIK3CA^{H1047R} oncoproteins modulate intestinal organoid phenotypes

To study processes after gain of oncogenic mutations in the Wnt–β-catenin and PI3K pathways in the intestinal epithelium, we generated transgenic mice carrying doxycycline-inducible oncogenes coexpressed with the fluorescent marker tdTomato in a modified Gt(ROSA26)Sor locus (Fig. 1 A; Vidigal et al., 2010). Four transgenic mouse lines were used, producing CTNNB1^{stab}, PIK3CA^{H1047R}, both oncoproteins together from a single transgene to ensure coexpression, or firefly luciferase as a negative control (for in vivo phenotypes, see Fig. S1).

To study CTNNB1^{stab} and PIK3CA^{H1047R} in vitro, we cultured intestinal organoids in a 3D Matrigel matrix and crypt culture medium (CCM) containing the growth factors R-spondin, EGF, and noggin (CCM-REN; Sato et al., 2011b). A modified medium lacking the Wnt cofactor R-spondin (CCM-EN) was used to select for organoid cells producing CTNNB1^{stab} alone or CTNNB1^{stab}–PIK3CA^{H1047R}. These represent the relevant oncogene combinations in CRC progression: β-catenin activation triggers adenoma formation, whereas the conversion to carcinoma frequently involves activation of both β-catenin and PI3KCA, among other alterations (The Cancer Genome Atlas Network, 2012).

In CCM-EN, CTNNB1^{stab}-induced cultures grew out as spheroids, devoid of crypt–villus organization (Fig. 1 B; Farrall et al., 2012). The CTNNB1^{stab}–PIK3CA^{H1074R} combination resulted in the formation of mixed phenotypes comprising organoids, spheroids, and colonies growing in 2D on the plastic surface. In contrast, PIK3CA^{H1047R} organoids died in CCM-EN.

Transcriptome analysis of CTNNB1^{stab} and PIK3CA^{H1047R} in intestinal cells

We first analyzed transcriptomes after induction of the oncoproteins. CTNNB1^{stab} induced or repressed 895 genes compared with 245 for PIK3CA^{H1047R}, and the combination of both oncoproteins regulated 784 additional genes (Fig. 1, C and D). We clustered the 1,000 most variable genes and annotated the clusters by gene ontology (Fig. 1 E; Huang et al., 2009). Clusters 2 and 3, repressed the most by the oncoprotein combination, were enriched for apoptosis regulators such as *Bcl2l11*. Clusters 4 and 5 were defined by genes promoting DNA replication and cell cycle progression. Cluster 4, induced specifically by CTNNB1^{stab}, included *Myc* and the stem cell marker *Lgr5*. Cluster 5, induced by both PIK3CA^{H1047R} and CTNNB1^{stab}, was enriched for cyclin and aurora kinase genes. Cluster 6 revealed a focus on protein biosynthesis, with many genes encoding tRNA synthases and ribosomal components.

We assigned molecular functions to the oncoproteins by gene set enrichment analysis (GSEA; Fig. 1 F; Subramanian et al., 2005). CTNNB1^{stab} and PIK3CA^{H1047R} specifically induced hallmark signatures comprising Wnt–β-catenin– and PI3K-AKT-mTOR–responsive genes, respectively. Both oncoproteins, alone and in combination, activated proliferation signatures comprised of MAPK targets (Jürchott et al., 2010), E2F targets, or mitosis-associated genes. Metabolic signatures related to the two main steps of energy production, glycolysis and oxidative phosphorylation, were more strongly induced by PIK3CA^{H1047R} as compared with CTNNB1^{stab}.

When we assessed cell type–specific transcriptional signatures (Merlos-Suárez et al., 2011), CTNNB1^{stab} and PIK3CA^{H1047R} both induced transiently amplifying cell-specific genes at the expense of differentiation-specific genes normally expressed in enterocytes. Yet only CTNNB1^{stab}, and not PIK3CA^{H1047R}, induced intestinal stem cell markers. Notably absent was the deregulation of genes implicated in the epithelial–mesenchymal transition (EMT).

PIK3CA^{H1047R} and CTNNB1^{stab} play specific roles in the regulation of apoptosis, clonogenicity, and metabolic adaptation

In line with the transcriptome analysis, we found that CTNNB1^{stab}- and PIK3CA^{H1047R}-induced organoid cells proliferated faster than controls. Induction of the oncoprotein combination resulted in even faster proliferation, as assessed by cell count, DNA content, and quantification of crypt domains per organoid (Fig. 2 A).

To test for resistance to apoptosis, we passaged CTNNB1^{stab}- and CTNNB1^{stab}–PIK3CA^{H1047R}-induced cultures as small cell clusters. Under these conditions, survival and outgrowth is limited by anoikis, a form of Rho kinase–dependent apoptosis (Sato et al., 2009). CTNNB1^{stab}-induced cultures had a low colony-forming capacity compared with cultures producing CTNNB1^{stab} and PIK3CA^{H1047R} (Fig. 2 B). Addition of the Rho kinase inhibitor Y-27632 during passage specifically increased the colony-forming capacity of CTNNB1^{stab} cultures. Thus, in agreement with the transcriptome analysis, the oncoprotein combination represses anoikis and promotes survival of intestinal cells.

We next assessed clonogenicity by reseeding single cell suspensions in the presence of Y-27632. In such assays, outgrowth is restricted to single cells maintaining stem cell traits in the absence of niche cells (Sato et al., 2011a). Limiting dilution assays showed that CTNNB1^{stab}- and CTNNB1^{stab}–PIK3CA^{H1047R}-induced cultures could be propagated by as few as 15 cells per well. In contrast, control and PIK3CA^{H1047R}-induced organoids could not be propagated even when seeding 150 individual cells per well (Fig. 2 C). Thus, PIK3CA^{H1047R} cannot compensate for β-catenin activity in the maintenance of intestinal stem cell function.

We tested activities of key glycolytic enzymes in wild-type cultures or after activation of the transgenes to follow up our finding of deregulated metabolic signatures. Aldolase and lactate dehydrogenase activities were reduced in CTNNB1^{stab}- and compound oncogene–expressing cultures (Fig. 2 D). Lower expression of *Aldob*, coding for aldolase, was also observed in the transcriptomes of CTNNB1^{stab}-induced and compound organoids. However, we were not able to detect changes in enzyme activities early after induction, probably because of lower fractions of induced cells at these time points (Fig. S2).

Levels of mitochondrial energy production, as assessed by a bioluminescence substrate conversion assay, were also affected by the induction of the oncoproteins. Short-term (24 h) transgene induction already increased oxidative phosphorylation in the PIK3CA^{H1047R}-producing and compound organoids, but not in CTNNB1^{stab}-producing organoids (Fig. 2 E). This agrees with the signatures found in the transcriptomes. After 6 d of induction, increased oxidative phosphorylation was detected in all oncoprotein-producing models (Fig. S2), suggesting that long-term processes like changes in cell fate also modulate oxidative phosphorylation.

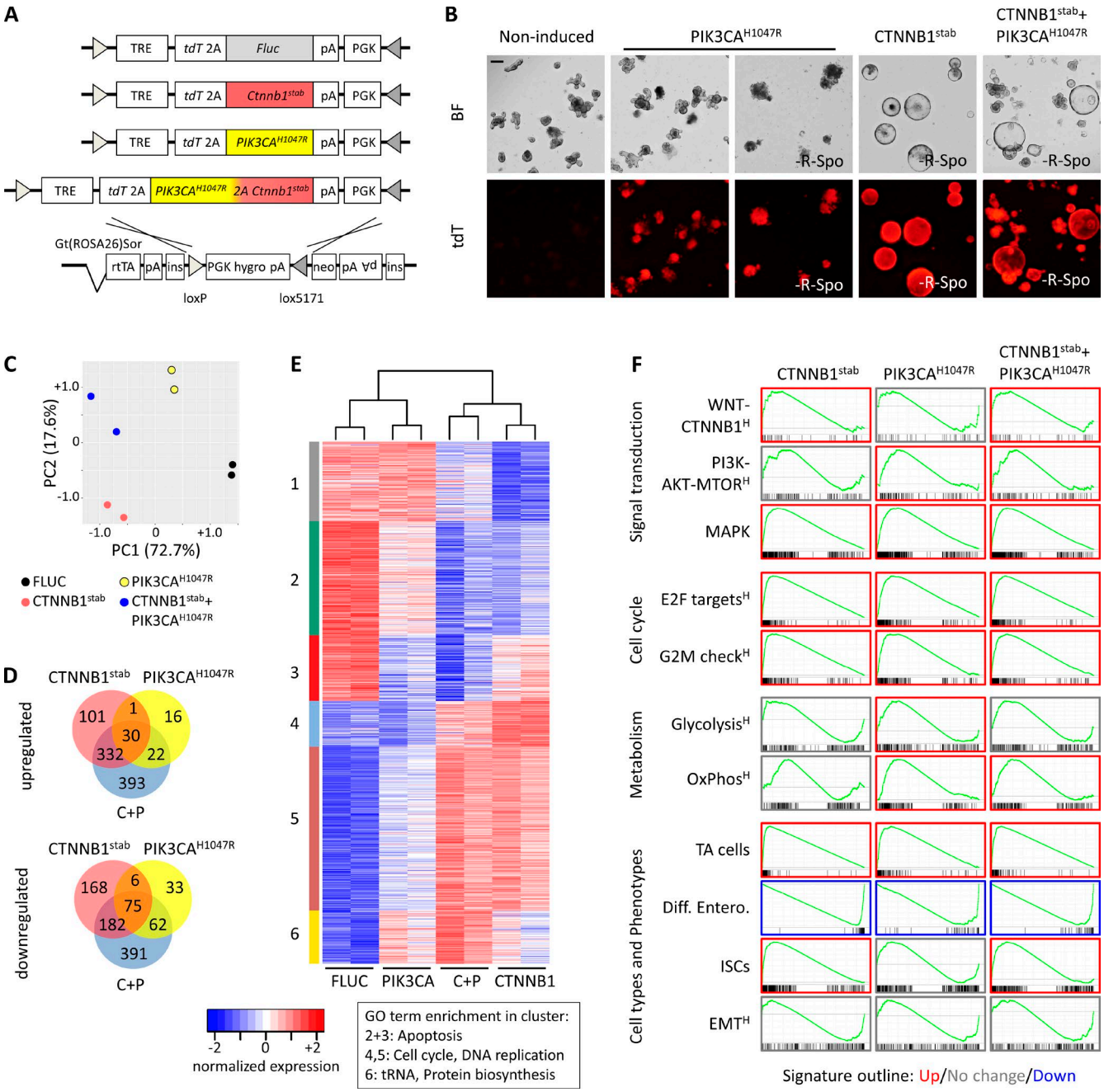

Figure 1. **Establishment and transcriptome analysis of intestinal organoids induced for CTNNB1^{stab} and/or PIK3CA^{H1047R}.** (A) Schematic representation of transgenes used. ins, chicken β-globin 1.2-kb insulator; neo, neomycine phosphotransferase; pA, polyadenylation signal; PGK, phosphoglycerate kinase promoter; rtTA, reverse tetracycline-controlled transactivator; tdT, tdTomato; TRE, tet-responsive element. (B) Phenotypes of organotypic cultures ± R-spondin (R-Spo), as indicated. Top, brightfield (BF) images; bottom, tdTomato (tdT) fluorescence. Bar, 200 µm. (C–F) Transcriptome analysis. (C) Principal component analysis. Principal components PC1 and PC2 and an explained variation are given. Fluc, firefly luciferase. (D) Venn diagrams of CTNNB1^{stab}- and PIK3CA^{H1047R}-induced (C+P) and repressed genes, as indicated. (E) Cluster analysis of the 1,000 most variable genes. Gene ontology (GO) term enrichment for clusters is indicated in the box. Blue, low expression; red, high expression. (F) GSEA analysis of the transcriptomes. ISC, intestinal stem cell; MAPK, mitogen-activated protein kinase; TA, transiently-amplifying.

CTNNB1^{stab} and PIK3CA^{H1047R} synergistically control intestinal cell attachment and motility

We frequently observed colonies attaching to the surface of the culture dish in the double CTNNB1^{stab}–PIK3CA^{H1047R}-induced cultures. To enforce contact between outgrowing organoids and the plastic surface, we embedded organoids in diluted (50%) Matrigel (Fig. 3, A and B). CTNNB1^{stab}–PIK3CA^{H1047R}-induced organoids frequently attached, whereas expression of the other transgenes favored growth in the 3D matrix. Stabilization of β-catenin by the GSK3β inhibitor CHIR99021 augmented colony attachment in single PIK3CA^{H1047R}-induced cultures, providing evidence for synergistic roles of PI3K and β-catenin in regulating cell attachment.

We seeded organoids directly into a culture dish with CCM-EN in the absence of Matrigel (Fig. 3 C). CTNNB1^{stab}-induced spheroids disintegrated and were strongly positive for cleaved caspase 3. In contrast, CTNNB1^{stab}–PIK3CA^{H1047R}-

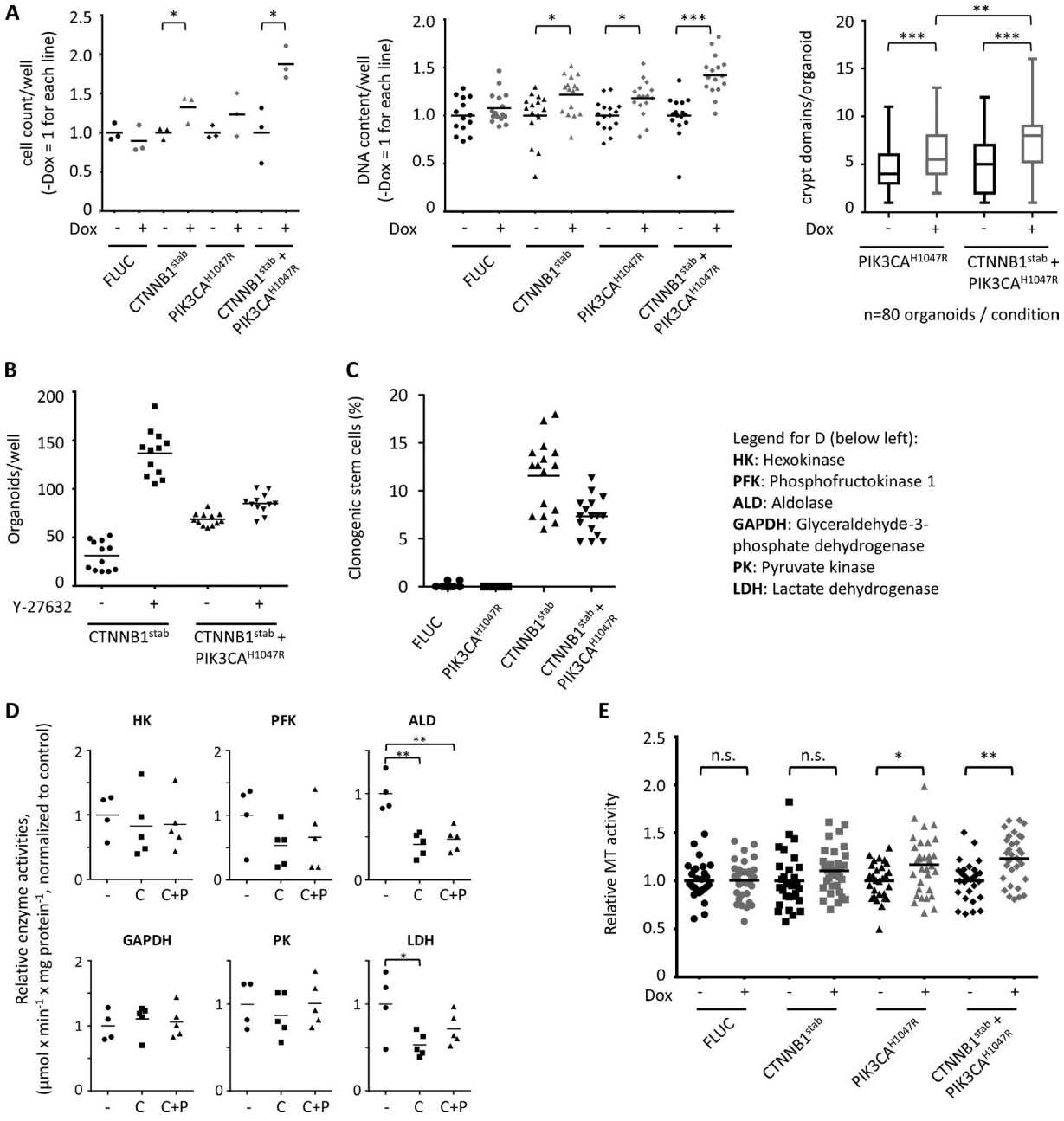

Figure 2. **PIK3CA^{H1047R} and CTNNB1^{stab} play specific roles in the regulation of proliferation, apoptosis, clonogenicity, and metabolism.** (A) Quantification of organoid proliferation, as indicated, after 4 d of induction. Cell numbers, DNA content, and crypt numbers are given. For the latter, bars and whiskers indicate median, 25th and 75th percentiles, and minimum/maximum values. (B) Passaging efficacy after disaggregation. Organoids per well after 4 d of outgrowth are given. (C) Clonogenicity after passaging of single cell suspensions. Organoids per well 8 d after seeding of 150 cells per well are given. (D) Quantification of key glycolytic enzyme activities in lysates of wild-type and long-term CTNNB1^{stab}- or CTNNB1^{stab}–PIK3CA^{H1047R}-induced cultures. C, CTNNB1^{stab}; C+P, CTNNB1^{stab}–PIK3CA^{H1047R}. (E) Quantification of oxidative phosphorylation using a mitochondrial metabolic (MT) assay 24 h after transgene induction, as indicated. Statistical analyses in all subfigures were obtained by two-tailed *t* tests. *, P < 0.05; **, P < 0.005; ***, P < 0.0005. Dox, doxycycline.

induced organoids grew out flat on the culture dish surface and were largely negative for cleaved caspase 3, demonstrating the antiapoptotic effect of additional PIK3CA^{H1074R}. Attached colonies were stained uniformly positive for E-cadherin and negative for N-cadherin, indicating their epithelial character.

We used time-lapse microscopy to follow growth of CTNNB1^{stab} and compound transgenic cultures in diluted Matrigel (Fig. 3 D and Videos 1, 2, and 3). CTNNB1^{stab}-induced spheroids proliferated continuously at fixed positions within the 3D matrix and rarely fused. In contrast, CTNNB1^{stab}–PIK3CA^{H1047R}-induced cultures showed a more complex behavior: First, as mentioned in the first section of Results and discussion, they displayed mixed organoid and spheroid phenotypes. Second, they frequently fused while proliferating. Third, colonies attaching to the surface were highly motile. The 2D cell clusters collectively moved toward each other and fused to form larger colonies. In summary, the in vitro analyses indicate that PIK3CA^{H1047R} in combination with activated Wnt–β-

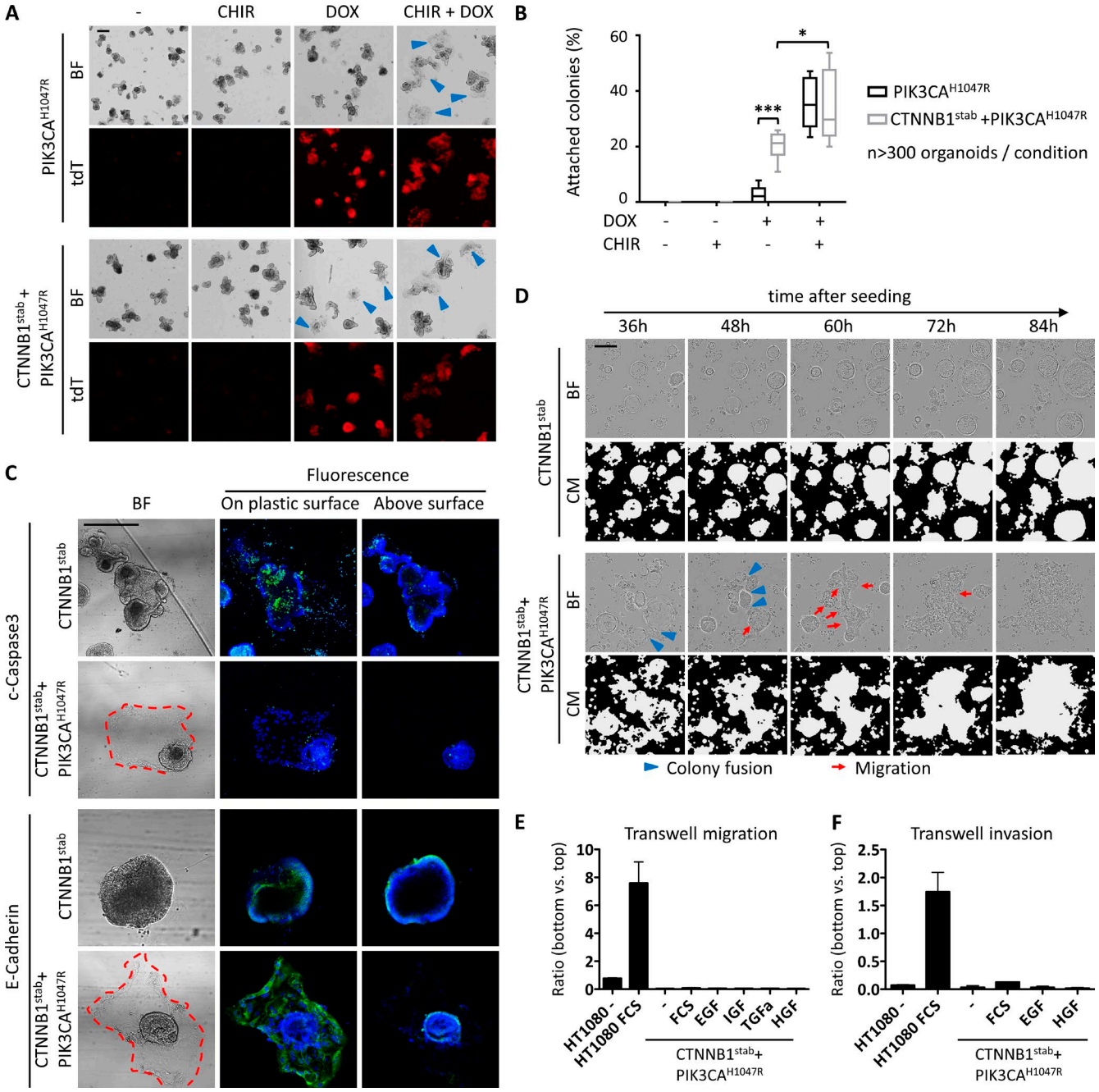

Figure 3. **CTNNB1^{stab} and PIK3CA^{H1047R} synergize in the induction of epithelial cell attachment and motility.** (A) Phenotypes of organotypic cultures induced for PIK3CA^{H1047R} or CTNNB1^{stab}–PIK3CA^{H1047R} or treated with the GSK3β inhibitor CHIR99021 (CHIR). Blue arrowheads indicate colonies growing in 2D on the surface. Top rows, brightfield (BF) images; bottom rows, tdTomato (tdT) fluorescence. (B) Quantification of 2D colonies as per A. Bars and whiskers indicate median, 25th and 75th percentiles, and minimum/maximum values. Statistical analysis was obtained by two-tailed *t* test. *, P < 0.05; ***, P < 0.0005. (C) Immunofluorescence images of CTNNB1^{stab} or CTNNB1^{stab}–PIK3CA^{H1047R}-induced cultures using Alexa Fluor 488–labeled α–cleaved caspase 3 (c-Caspase3) or α–E-cadherin antibodies. Brightfield and fluorescence channels are given. Nuclei are in blue. Red dashed lines demarcate edges of colonies. (D) Still images from time-lapse videos of organotypic cultures, as indicated. Top, brightfield images; bottom, confluence masks (CMs) showing areas with cells. Blue arrowheads indicate fusing colonies; red arrows indicate migrating cell clusters. Bars, 200 µm. (E and F) Quantification of transwell migration (E) and transwell invasion (F) assays. Red fluorescent object counts on the top in relation to the bottom of the porous membrane 4 d after the start of the assay. Graphs show means and SD of four assays.

catenin induces cell attachment, spreading, and motility in intestinal epithelial cells.

We tested CTNNB1^{stab}–PIK3CA^{H1047R}-induced cultures for chemotaxis and invasiveness through a porous membrane toward gradients of 10% FCS or the growth factors EGF and TGFα (both EGF receptor ligands), insulin-like growth factor (IGF; an IGF receptor ligand) or hepatocyte growth factor (binding the c-Met receptor), but we could detect neither (Fig. 3, E and F). We attribute the failure of CTNNB1^{stab}–PIK3CA^{H1047R}-induced intestinal cells to invade to a lack of chemotactic response to the growth factors and to their collective form of cell migration, which is likely incompatible with invasion through outlets at the basal side of a cell cluster.

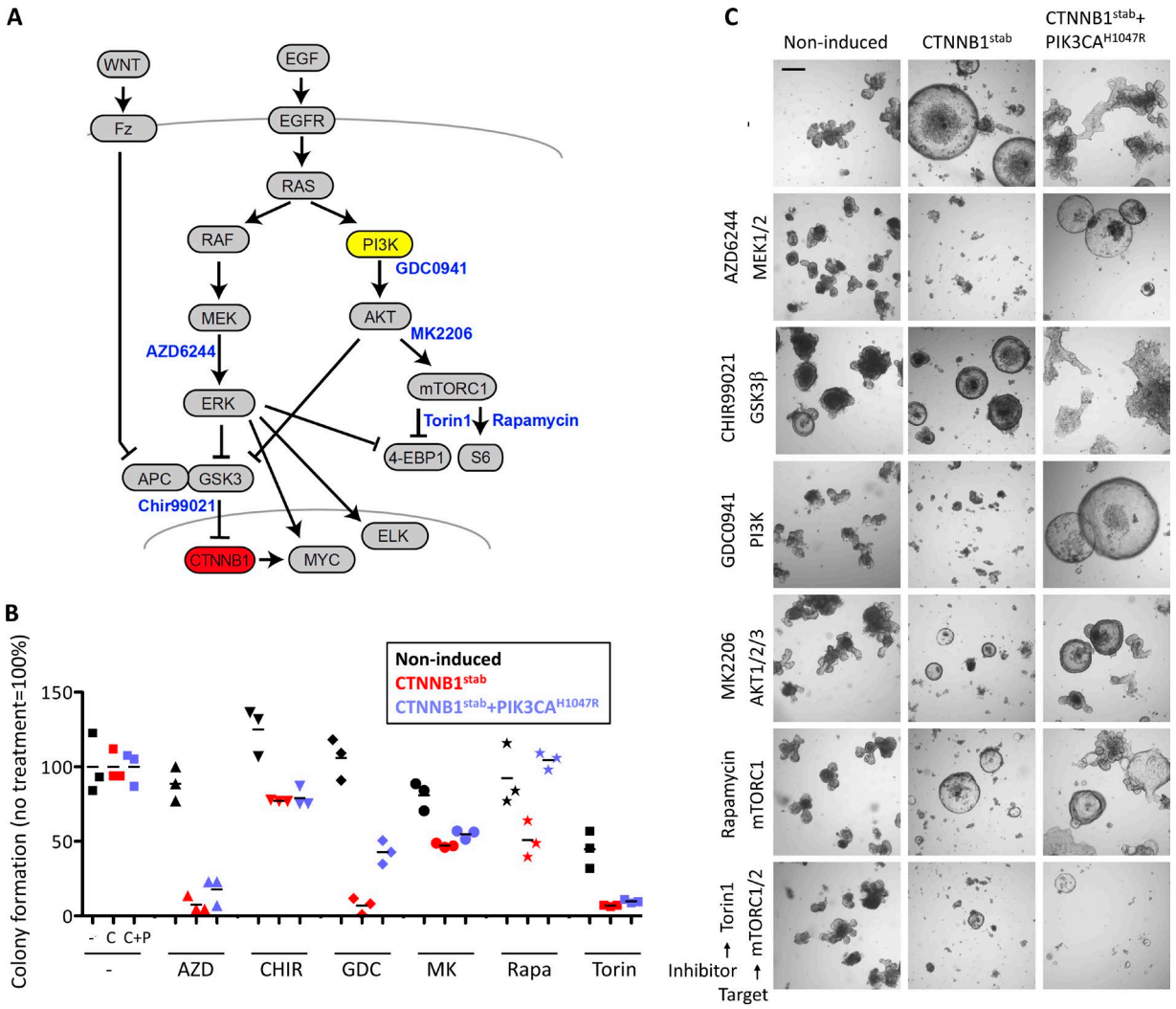

Figure 4. **Network perturbation analysis links oncogenic signal transduction to organoid survival.** (A) Schematic representation of the cell signal transduction network under investigation. Inhibitors are given in blue. Rapamycin specifically inhibits the mTORC1–S6K interaction, whereas Torin1 in addition inhibits the mTORC1–4EBP1 interaction and mTORC2 activities. Fz, Frizzled; RAF, rapidly accelerated fibrosarcoma; RAS, rat sarcoma. (B) Colony-forming capacity of wild-type, CTNNB1^{stab}- or CTNNB1^{stab}–PIK3CA^{H1047R}-induced organotypic cultures in the presence of the indicated inhibitors. AZD, AZD6244; C, CTNNB1^{stab}; C+P, CTNNB1^{stab}–PIK3CA^{H1047R}; CHIR, CHIR99021; GDC, GDC0941; MK, MK2206; Rapa, rapamycin; (C) Phenotypes of organotypic cultures in the presence of the indicated inhibitors or solvent control (indicated by dash). Bar, 200 µm.

Previous studies in CRC cell lines (Samuels et al., 2005) and mouse models (He et al., 2007; Leystra et al., 2012; Deming et al., 2014; Hare et al., 2014) found that oncogenic PIK3CA in conjunction with activated β-catenin can contribute to invasiveness. We conclude from our experiments that the CTNNB1^{stab} and PIK3CA^{H1047R} oncoproteins are not sufficient on their own to induce invasiveness or EMT in intestinal organoids.

Perturbation of the β-catenin–MAPK–PI3K network reveals the specific vulnerabilities of oncogene-induced organoid cultures

To assess the roles of specific nodes of the cell signaling network in establishing cancer-associated organoid phenotypes, we used a panel of pharmaceutical inhibitors. These were directed against MAPK kinase (MEK; AZD6244; Yeh et al., 2007), Class I PI3K (GDC0941; Folkes et al., 2008), AKT (MK2206; Hirai et al., 2010), different activities of the mTOR complexes (rapamycin and Torin1; Thoreen and Sabatini, 2009), and GSK3β (CHIR99021; Bennett et al., 2002; Ring et al., 2003; see Fig. 4 A for a network diagram). Inhibitors were used at concentrations that allowed survival of wild-type organoids for at least 3 d.

We quantified the colony-forming capacity of transgenic cultures in the presence of inhibitors. GDC0941 and rapamycin specifically inhibited the outgrowth of CTNNB1^{stab}-induced cultures but not of those expressing the combination with PIK3CA^{H1047R} (Fig. 4 B). AZD6244 and Torin1 strongly blocked colony formation in both transgenic models. Our inhibitor assays suggest the existence of a transient sensitivity of adenomatous cells exhibiting high β-catenin activity to rapamycin, in line with a previous finding in APC-deficient intestinal cells (Faller et al., 2014). We find here that resistance to rapamycin is restored by the acquisition of the PIK3CA^{H1047R} mutation.

We also evaluated further phenotypes of the cultures (Fig. 4 C). Wild-type organoids displayed few discernible changes upon any inhibitor treatment except for CHIR99021, which mediated the formation of enlarged crypt domains. In contrast to CTNNB1^{stab}-induced cultures, which generally

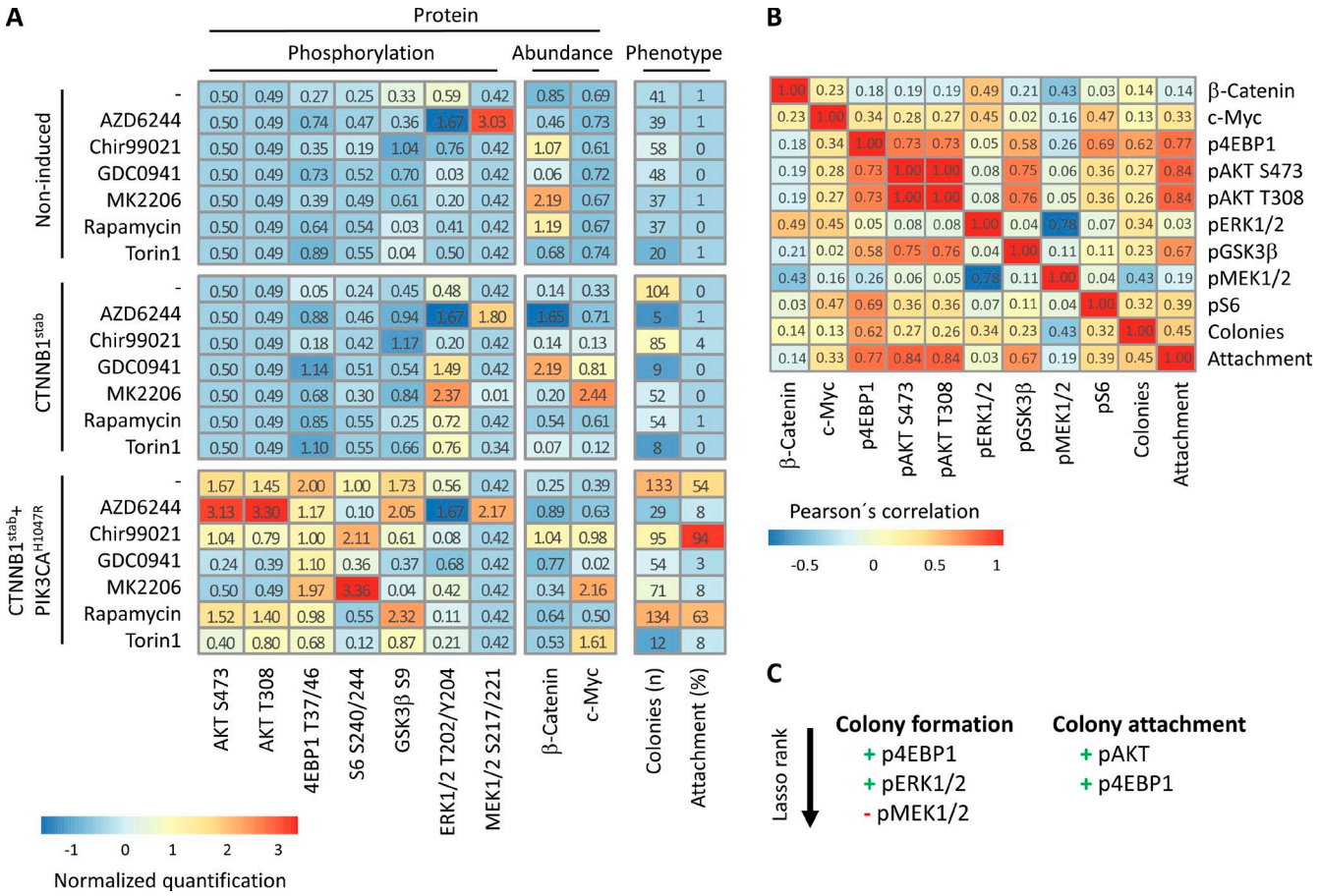

Figure 5. **Network quantification identifies 4EBP1 and AKT as key nodes for colony outgrowth and cell motility.** (A) Data matrix of protein/phosphoprotein and phenotypic analysis. For proteins/phosphoproteins, normalized linear values are given. Phenotypes are given as absolute numbers (colonies) or percent surface covered (2D growth). Dash indicates solvent control. (B) Pearson's correlation matrix of protein/phosphoprotein and phenotypic data. Positive values (red) indicate positive correlation, negative values (blue) indicate anticorrelation. (C) Most relevant proteins/phosphoproteins for predicting phenotypes, as determined by Lasso. Also see Fig. S3.

formed spheroids without higher-order structures, double CTNNB1^{stab}–PIK3CA^{H1047R} cultures displayed a diverse array of phenotypes, as detailed in the first section of the Results and discussion. In the presence of MEK and PIK3CA inhibitors, spheroids formed preferentially, whereas inhibition of GSK3β favored the formation of 2D cell clusters.

Quantification of the β-catenin–MAPK–PI3K network reveals signaling nodes associated with phenotypic switches

To link states of the cell signaling network to oncoprotein activities, we quantified proteins/phosphoproteins in control and long-term induced CTNNB1^{stab} or CTNNB1^{stab}–PIK3CA^{H1047R} organoids and inhibitor treatments for 24 h (Fig. 5 A). Phosphorylation levels of key signaling nodes AKT^{S473}, AKT^{T308}, 4EBP1$^{T37/T46}$, S6$^{S240/S244}$, GSK3β^{S9}, extracellular signal-related kinase (ERK) 1$^{T202/Y204}$ and ERK2$^{T185/Y187}$ (ERK1/2$^{T202/Y204}$), and MEK1/2$^{S217/S221}$, and the abundance of two transcription regulators (β-catenin and c-Myc) were measured. Induction of CTNNB1^{stab} alone did not significantly alter the phosphorylation of the analyzed proteins. Induction of CTNNB1^{stab}–PIK3CA^{H1074R} resulted in the phosphorylation of AKT, the direct AKT kinase target GSK3β^{S9}, and the AKT-mTORC1 target sites in 4EBP1 and S6 (see Fig. 4 A for a network diagram; Cross et al., 1995; Song et al., 2012). Inhibitor treatment perturbed signal transduction and uncovered key features of the network: negative feedback from ERK to MEK (Dougherty et al., 2005; Fritsche-Guenther et al., 2011) was found regardless of oncogene activation, resulting in phospho-ERK depletion but phospho-MEK accumulation upon ADZ6244 treatment. We also observed bidirectional negative feedback between AKT and ERK (Rommel et al., 1999; Zimmermann and Moelling, 1999; Fritsche-Guenther et al., 2016). Blockade of the PI3K–AKT axis by GDC0941 or MK2206 resulted in higher phosphorylation levels of ERK in CTNNB1^{stab}-induced spheroids but not in normal organoids. Thus, AKT-to-ERK feedback appears to depend on oncogenic activation of β-catenin in intestinal cells. Inhibition of PI3K or AKT after induction of both oncoproteins expectedly reduced phosphorylation of the AKT target GSK3β^{S9} but unexpectedly did not abrogate phosphorylation in the downstream targets 4EBP1 and S6. It thus appears that AKT and mTORC1 can be uncoupled in this setting.

We found that CTNNB1^{stab}- and CTNNB1^{stab}–PIK3CA^{H1047R}-induced cultures, under most conditions, displayed higher levels of c-Myc, which is known to be a β-catenin target (He et al., 1998). However, the signal was at the lower detection limit in our capillary protein assays, precluding a meaningful interpretation across all conditions.

We finally correlated the protein/phosphoprotein analyses with the cell phenotypes quantified as colony numbers and

2D outgrowth using Pearson's correlation (Fig. 5 B). Colony formation and thus cell survival was best correlated with phosphorylation levels of 4EBP1 across all measurements. In contrast, cell attachment and motility was linked most strongly to AKT phosphorylation and only to a lesser extent to phosphorylation levels of 4EBP1 and GSK3β. Likewise, Lasso regression (Tibshirani, 1996) selected 4EBP1 and AKT as the phosphoproteins most strongly related to colony number and the formation of motile 2D colonies, respectively (Figs. 5 C and S3).

Our study links cancer-related phenotypes to the cell signaling network in intestinal organoids. 4EBP1 has previously been identified as a converging point of MEK–ERK and PI3K–AKT signals for cancer cell survival (She et al., 2010), and our analysis is in line with such a key role. We show that oncogenic β-catenin and PI3K activities interact in the acquisition of multiple cancer-related phenotypes in organoids grown in Matrigel. A more complex microenvironment composed of many matrix proteins and cell types could play unappreciated key roles in CRC in vivo to induce or repress further cancer phenotypes, such as invasion or EMT, in response to oncogenic signals (Bissell and Hines, 2011).

Materials and methods

Generation of transgenic mice

Transgene cassettes were constructed by linking tdTomato to human $PIK3CA^{H1047R}$ and/or murine stabilized mutant $CTNNB1^{stab}$ (S33A, S37A, T41A, and S45A) or firefly luciferase via 2A peptides and then subsequently cloning these gene combinations into a doxycycline-inducible expression cassette. Transgenes contained a phosphoglycerate kinase promoter and were flanked by heterologous loxP and lox5171 sites. Transgenes were integrated by Cre recombinase–mediated cassette exchange into a previously modified Gt(ROSA)26Sor locus harboring a promoterless neomycin resistance gene in F1 hybrid B6/129S6 embryonic stem cells (Fig. 1 A). Recombined clones were selected by 250 µg/ml G418 and analyzed by Southern blotting of genomic DNA digested with BamH1 and HindIII, using the neomycin cassette as a probe (Vidigal et al., 2010). Animals were generated by diploid aggregation, housed at a 12:12 h light/dark cycle, and fed ad libitum. Transgenes were induced by administration of 4 mg/ml doxycycline provided in a 5% sucrose solution via drinking water. Mouse lines were inbred to C57/BL6. Transgenic animal production and experimentation was approved by the Berlin State Office for Health and Social Affairs (G0185/09 and G0143/14).

Organoid culture and phenotypic analysis

Organoid cultures were initiated and propagated as described by Sato et al. (2011b) using 48-well plates with 15-µl droplets of medium and Matrigel (BD) per well overlaid with 300 µl CCM-REN. Crypt culture media were exchanged every other day. All comparisons between $CTNNB1^{stab}$- and double $CTNNB1^{stab}$–$PIK3CA^{H1047R}$-induced cultures were done using CCM-EN + 2 µg/ml doxycycline. When we additionally used $PIK3CA^{H1047R}$-producing organoids in functional assays, we cultured all models in the presence of R-spondin (CCM-REN + doxycycline), resulting in inconsistent transgene expression, i.e., the presence of a fraction of noninduced cells. Images of cultures were taken with a Biozero microscope using a Plan Fluor extra-long working distance DM 20× C 0.45 NA objective and Biozero observation and Analyser software (Keyence).

The following growth factors, inducers, and small-molecule inhibitors were used: EGF (50 ng/ml; PeproTech), insulin-like growth factor (100 ng/ml; PeproTech), hepatocyte growth factor (50 ng/ml; PeproTech), TGFα (10 ng/ml; PeproTech), noggin (100 ng/ml; PeproTech); doxycycline (2 µg/ml; Sigma-Aldrich), Y-27632 (10 µM; Sigma-Aldrich), AZD6244 (10 µM; SelleckChem), GDC0941 (1 µM; SelleckChem), CHIR99021 (6 µM; SelleckChem), MK2206 (250 nM; SelleckChem), rapamycin (100 nM; SelleckChem), and Torin1 (4 µM; SelleckChem). Stocks were dissolved in either 70% EtOH (doxycycline), *N*-methyl-2-pyrrolidon (Torin1), or DMSO (all others), and solvent concentrations were kept uniform across all wells in the experiments. Sublethal concentrations for inhibitors for cell signal transduction were determined in noninduced cultures. For signal inhibition experiments, inhibitors were added to already doxycycline-induced cultures.

For quantification of organoid proliferation, cultures were induced for 4 d. Cells were counted in well multiples after disaggregation using a Neubauer chamber. DNA content was determined using components of the CellTox Green Cytotoxicity Assay (G8741; Promega) as given in the Metabolic assays section. For clonogenicity assays, 15 or 150 cells per well were seeded into Matrigel domes in 48-well plates with CCM-REN + Y27632, and organoid colonies were counted after 8 d. To systematically analyze the 2D attachment phenotype, cultures were disaggregated, seeded in 50% Matrigel onto precooled culture plates, and transferred to 37°C after 5 min. Time-lapse assays were performed in an Incucyte Zoom device (Essen Bioscience) using the 10× objective and the phase contrast and red fluorescent channels. Organoid colony outgrowth and survival were quantified from time-lapse videos from >3 wells per condition, and only colonies that survived for 4 d were counted. Colonies fusing during the examination period were counted as separate colonies. Transwell motility and invasion assays were performed with a Chemotaxis system (IncuCyte ClearView 96-Well Chemotaxis Plate; 4582; Essen Bioscience) as per manufacturers' application note. Wells were coated with 50 µg/ml Matrigel. Pore size of the transwell plates was 8 µM.

Protein analysis

For protein/phosphoprotein analysis from organoids, a WES capillary Western system (12–230 kD Master kit α-Rabbit–HRP; PS-MK01; Protein Simple) was used. In brief, organoids were collected in cold PBS and spun down, and Matrigel was removed. Organoids were taken up in 25-µl M-Per lysis buffer (78501; Thermo Fisher Scientific) supplemented with phosphatase and proteinase inhibitors (PhosSTOP EASYpack phosphatase inhibitor cocktail tablets; 04906837001; and Complete EDTA-free phosphatase inhibitor tablets; 11873580001; Roche), left on ice for 30 min, and subsequently frozen at −80°C. After thawing, samples were sonicated and spun down, and the protein content of the supernatants was determined by bicinchoninic acid (BCA) assays. Depending on the size of the analyte, either cofilin or vinculin were used to normalize the readout from each capillary. The following rabbit-derived antibodies were used: $pAKT^{T308}$ (1:50; 2965), $pAKT^{S473}$ (1:50; 9271), $pGSK3\beta^{S9}$ (1:50; 9336), $pS6RB^{S240/S244}$ (1:50; 5364), $p4EBP1^{T37/T46}$, (1:50; 2855), $pERK1/2^{T202/Y204}$ (1:50; 9101), $pMEK1/2^{S217/S221}$ (1:50; 9121), β-catenin (1:50; 9562), cofilin (1:50; 5175), and vinculin (1:30; 4650; Cell Signaling Technology). c-Myc (1:50; ab32072) was purchased from Abcam. Three biological replicates were used per condition.

For immunohistochemical stainings, tissues were fixed in 4% formaldehyde, dehydrated in a graded ethanol series, embedded in paraffin, and sectioned at 4 µm. Sections were hydrated, antigens were retrieved by boiling in Tris-buffered 1.2 mM EDTA, pH 9.0, for 20 min, and sections were blocked by 1% BSA in PBS. We used the following rabbit-derived antibodies: anti-KI67 (1:200; ab16667; Abcam), anti-RFP (1:200; 600-401-379; Rockland), and anti–cleaved caspase

3 (1:300; 9661; Cell Signaling Technology). Signals were detected using ImmPRESS secondary antibodies and the NOVAred substrate kit (Vector Laboratories).

Immunofluorescent staining of CTNNB1^{stab} and CTNNB1^{stab}–PIK3CA^{H1047R} cultures was done from cultures growing for 2 d on multiwell slides (80826; Ibidi) in the absence of Matrigel. For microscopy, cultures were washed with PBS, fixed with 4% formaldehyde/PBS for 15 min at room temperature, permeabilized with 0.5% Triton X-100/PBS for 5 min, blocked with DMEM/10% FCS for 30 min, and incubated with the first antibody diluted in 150 µl/well DMEM/10% FCS at 4°C in a wet chamber overnight. The following antibodies were used: anti–E-cadherin (1:250; 3195; Cell Signaling Technology), anti–cleaved caspase 3 (1:400; 9664; Cell Signaling Technology), and goat anti–rabbit Alexa Fluor 488 (1:1,000; A11008; Thermo Fisher Scientific). Images were taken with an LSM710 nonlinear optical AxioObserver microscope using a Plan-Apochromat 10× 0.3 M27 objective and Zen software (ZEISS).

Metabolic analyses

Enzyme activity assays were determined from organoid cell extracts. Cells were collected in PBS supplemented with Complete Phosphatase Inhibitor Cocktail 2 and Phosphatase Inhibitor Cocktail 3 (Sigma-Aldrich) and then were lysed by freezing. Samples were thawed and centrifuged for 10 min at 21,000 *g* at 4°C, and supernatant was used for the assays. All enzyme activities were measured in freshly prepared extracts at 37°C in a Synergy H4 plate reader (BioTek). Protein determinations were performed with the BCA Protein Assay kit (Thermo Fisher Scientific). A standard assay buffer containing 0.1 Tris-HCl, pH 7.0, 15 mM NaCl, 0.5 mM CaCl, 140 mM KCl, and 5 mM phosphate buffer, pH 7.0, was used. For all assays, the reaction mixtures without start reagents were prewarmed at 37°C. Composition of the reaction mixtures were as follows: hexokinase (enzyme commission [EC] 2.7.1.1) – 10.5 mM $MgSO_4$, 1.2 mM $NADP^+$, 10 mM glucose, 1.75 U/ml glucose-6-phosphate dehydrogenase, and 10 mM ATP (the production of NADPH was monitored over time by measuring absorbance at 340 nm); phosphofructokinase 1 (EC 2.7.1.11) – 1.5 mM $MgSO_4$, 1.5 mM nicotinamide adenine dinucleotide (NADH), 1 mM ATP, 0.5 U/ml aldolase, 0.3 U/ml glycerol-3-phosphate dehydrogenase, 0.9 U/ml triosephosphate isomerase, and 2 mM fructose 6-phosphate (the consumption of NADH was monitored over time by measuring absorbance at 340 nm); aldolase (EC 4.1.2.13) – 0.5 mM $MgSO_4$, 1.5 mM NADH, 0.3 U/ml glycerol-3-phosphate dehydrogenase, 0.9 U/ml triosephosphate isomerase, and 2 mM fructose 1,6-bisphosphate (the consumption of NADH was monitored over time by measuring absorbance at 340 nm); GAPDH (EC 1.2.1.12) – 1 mM DTT, 1.5 mM $MgSO_4$, 1 mM ATP, 1.5 mM NADH, 22.5 U/ml 3-phosphoglycerate kinase, and 5 mM 3-phosphoglyceric acid (the consumption of NADH was monitored over time by measuring absorbance at 340 nm); pyruvate kinase (EC 2.7.1.40) – 1.5 mM $MgSO_4$, 1 mM ADP, 1 mM fructose 1,6-bisphosphate, 1.5 mM NADH, 50 U/ml lactate dehydrogenase, and 2 mM phosphoenolpyruvate (the consumption of NADH was monitored over time by measuring absorbance at 340 nm); and lactate dehydrogenase (EC 1.1.1.27) – 0.5 mM $MgSO_4$, 1.5 mM NADH, and 1 mM pyruvate (the consumption of NADH was monitored over time by measuring absorbance at 340 nm. Four different dilutions in PBS supplemented with the cocktails were analyzed to check for linearity.

Mitochondrial metabolic activity was measured using the RealTime Glo MT Cell Viability Assay (G9711; Promega). In short, organoids were passaged the day before the assay into a black-walled 96-well plate (3603; Corning). The next day, organoids were overlaid with 100 µl medium containing 0.1 µl NanoLuc enzyme, 0.1 µl MT Cell Viability Substrate, and 0.1 µl CellTox Green dye (G8741; Promega). Measurements of substrate conversion were performed using a Synergy 2 microplate reader (BioTek) set to 37°C. Luminescence was measured for 1 s, and fluorescence excitation and emission wavelengths were 485/20 and 528/20 nm, respectively. Measurements were done every hour, and mean values of three readouts were calculated. For normalization by DNA content, 5 µl of lysis solution (component of CellTox Green Cytotoxicity Assay; G8741; Promega) were added to each well. The plate was measured after 1 h of incubation at 37°C and 5% CO_2, and visual inspection was used for complete lysis.

RNA analysis

For RNA sequencing, organoids were induced for 24 h with 2 µg/ml doxycycline in CCM-REN medium. Fluorescence-activated cell sorting of induced cell populations was done after dissociation in TrypLE (Gibco) and 100 U/µl DNaseI (Sigma-Aldrich) for 15 min at 37°C followed by filtering through a 30-µM strainer (Costar) using an ARIA II Special Order Research Product (BD). Total RNA from sorted cells was extracted using the RNeasy Micro kit (QIAGEN), and 100 ng total RNA were used for library preparation with the ScriptSeq kit (Illumina) according to the manufacturer's instructions. 7–10 × 10^7 50-bp paired end reads per library were generated with a HiSeq 2500 sequencer (Illumina). Mapping and further processing is described in the next section. RNA-seq data are available in the GEO repository under accession no. GSE93947.

Olfm4 RNA in situ hybridization was performed on rehydrated paraffin sections using 800 ng/ml digoxigenin-labeled *Olfm4* antisense probes. Signals were detected using anti–digoxigenin-Fab fragments coupled to alkaline phosphatase (1:1,000; Roche) and a nitro blue tetrazolium and 5-bromo-4-chloro-3′-indolyphosphate chromogenic reaction. Primer sequences flanking the in situ probe were Olfm4 _s, 5′-GGACCTGCCAGTGTTCTGTT-3′; and Olfm4_ as_T7, 5′-TAA TACGACTCACTATAGGGCCCCCATTGTACCAATTCAC-3′.

Bioinformatics and statistical analyses

RNA-seq reads were aligned to the mouse genome GRCm38 using STAR aligner and Gencode exon annotations. Read counts were calculated for each gene ID using HTSeq. After removal of ribosomal reads, raw counts were normalized using the DESeq function EstimateSizeFactors, and dispersion in replicates was calculated using the DESeq function EstimateDispersions with default parameters. After removing lowly expressed genes with mean read counts below 64, data were log2 transformed, and the top 1,000 varying genes were selected by dividing the overall SD by the mean relative SD estimated by DESeq. K-means clustering was performed in R (nstart = 100 liters; max = 100) with six centers on genewise z-normalized expression of the top 1,000 varying genes. GSEA was done as previously described by Subramanian et al. (2005). Signatures are referenced in the main text or were taken from the Broad Institute Hallmark signature collection (Liberzon et al., 2015).

For correlation analyses, we computed the median of repeated protein and phosphoprotein measurements and set undetectable levels to 0. In total, nine proteins/phosphoproteins and two phenotypic responses were measured for 21 different conditions, corresponding with three oncogenic states and seven drug perturbations. To investigate the relationship between signaling state and phenotypic response as well as between individual proteins/phosphoproteins, we first computed the Pearson's correlation matrix between all measured entities for logarithmized (log(1 + x)) data. Next, to find a direct relationship between signaling state and phenotypic response, we used Lasso modeling (Tibshirani, 1996) to fit a linear model from the logarithmized and normalized protein/phosphoprotein data to phenotypic data. By using

an increasing penalty term for the linear model coefficient, proteins/phosphoproteins were ranked according to their importance.

Pairwise data comparisons were done using two-tailed *t* tests in Prism (GraphPad Software). For all figures, the following p-value cutoffs were used: *, $P < 0.05$; **, $P < 0.005$; ***, $P < 0.0005$. In cases where a range is given, we used the SD. For all parametric tests, we assumed normal data distribution, but this was not formally tested.

Online supplemental material

Fig. S1 shows synergy of CTNNB1^{stab} and PIK3CA^{H1047R} in inducing intestinal epithelial proliferation in vivo. Fig. S2 shows metabolic activities in intestinal organoids after the induction of transgenes. Fig. S3 shows LASSO fits for both numbers of colonies and colony attachment. Video 1 shows noninduced organoid cultures embedded in 50% Matrigel. Video 2 shows CTNNB1^{stab}-induced cultures embedded in 50% Matrigel. Video 3 shows CTNNB1^{stab}–PIK3CA^{H1047R}-induced cultures embedded in 50% Matrigel.

Acknowledgments

The authors acknowledge Silvia Schulze (Charité Universitätsmedizin Berlin) and Gaby Bläβ (Max Planck Institute for Molecular Genetics, Berlin) for excellent technical assistance and Sonja Banko (Max Planck Institute for Molecular Genetics animal facility, Berlin) for mouse care and management.

This work was in part funded by the Deutsche Forschungsgemeinschaft (grant MO2783/2-1 to M. Morkel), the German Ministry of Education and Research (grant eBio-0316184A to C. Sers and M. Morkel), and the German Cancer Consortium (DKTK) to C. Sers.

The authors declare no competing financial interests.

Author contributions: P. Riemer, M. Marks, K. van Eunen, and M. Morkel conducted, analyzed, and interpreted experiments; M. Rydenfelt and N. Blüthgen provided bioinformatic analyses; P. Riemer, K. Thedieck, B.G. Herrmann, C. Sers, and M. Morkel contributed to conception and design of the study; P. Riemer and M. Morkel wrote the manuscript.

Submitted: 18 October 2016
Revised: 8 February 2017
Accepted: 30 March 2017

References

Bennett, C.N., S.E. Ross, K.A. Longo, L. Bajnok, N. Hemati, K.W. Johnson, S.D. Harrison, and O.A. MacDougald. 2002. Regulation of Wnt signaling during adipogenesis. *J. Biol. Chem.* 277:30998–31004. http://dx.doi.org/10.1074/jbc.M204527200

Bissell, M.J., and W.C. Hines. 2011. Why don't we get more cancer? A proposed role of the microenvironment in restraining cancer progression. *Nat. Med.* 17:320–329. http://dx.doi.org/10.1038/nm.2328

Clevers, H., K.M. Loh, and R. Nusse. 2014. An integral program for tissue renewal and regeneration: Wnt signaling and stem cell control. *Science.* 346:1248012. http://dx.doi.org/10.1126/science.1248012

Cross, D.A., D.R. Alessi, P. Cohen, M. Andjelkovich, and B.A. Hemmings. 1995. Inhibition of glycogen synthase kinase-3 by insulin mediated by protein kinase B. *Nature.* 378:785–789. http://dx.doi.org/10.1038/378785a0

Deming, D.A., A.A. Leystra, L. Nettekoven, C. Sievers, D. Miller, M. Middlebrooks, L. Clipson, D. Albrecht, J. Bacher, M.K. Washington, et al. 2014. PIK3CA and APC mutations are synergistic in the development of intestinal cancers. *Oncogene.* 33:2245–2254. http://dx.doi.org/10.1038/onc.2013.167

Dougherty, M.K., J. Müller, D.A. Ritt, M. Zhou, X.Z. Zhou, T.D. Copeland, T.P. Conrads, T.D. Veenstra, K.P. Lu, and D.K. Morrison. 2005. Regulation of Raf-1 by direct feedback phosphorylation. *Mol. Cell.* 17:215–224. http://dx.doi.org/10.1016/j.molcel.2004.11.055

Faller, W.J., T.J. Jackson, J.R.P. Knight, R.A. Ridgway, T. Jamieson, S.A. Karim, C. Jones, S. Radulescu, D.J. Huels, K.B. Myant, et al. 2014. mTORC1-mediated translational elongation limits intestinal tumour initiation and growth. *Nature.* 517:497–500. http://dx.doi.org/10.1038/nature13896

Farrall, A.L., P. Riemer, M. Leushacke, A. Sreekumar, C. Grimm, B.G. Herrmann, and M. Morkel. 2012. Wnt and BMP signals control intestinal adenoma cell fates. *Int. J. Cancer.* 131:2242–2252.

Fearon, E.R. 2011. Molecular genetics of colorectal cancer. *Annu. Rev. Pathol.* 6:479–507. http://dx.doi.org/10.1146/annurev-pathol-011110-130235

Folkes, A.J., K. Ahmadi, W.K. Alderton, S. Alix, S.J. Baker, G. Box, I.S. Chuckowree, P.A. Clarke, P. Depledge, S.A. Eccles, et al. 2008. The identification of 2-(1*H*-Indazol-4-yl)-6-(4-methanesulfonyl-piperazin-1-ylmethyl)-4-morpholin-4-yl-thieno[3,2-*d*]pyrimidine (GDC-0941) as a potent, selective, orally bioavailable inhibitor of class I PI3 kinase for the treatment of cancer. *J. Med. Chem.* 51:5522–5532. http://dx.doi.org/10.1021/jm800295d

Fritsche-Guenther, R., F. Witzel, A. Sieber, R. Herr, N. Schmidt, S. Braun, T. Brummer, C. Sers, and N. Blüthgen. 2011. Strong negative feedback from Erk to Raf confers robustness to MAPK signalling. *Mol. Syst. Biol.* 7:489. http://dx.doi.org/10.1038/msb.2011.27

Fritsche-Guenther, R., F. Witzel, S. Kempa, T. Brummer, C. Sers, and N. Blüthgen. 2016. Effects of RAF inhibitors on PI3K/AKT signalling depend on mutational status of the RAS/RAF signalling axis. *Oncotarget.* 7:7960–7969.

Hare, L.M., T.J. Phesse, P.M. Waring, K.G. Montgomery, K.M. Kinross, K. Mills, V. Roh, J.K. Heath, R.G. Ramsay, M. Ernst, and W.A. Phillips. 2014. Physiological expression of the PI3K-activating mutation Pik3ca^{H1047R} combines with Apc loss to promote development of invasive intestinal adenocarcinomas in mice. *Biochem. J.* 458:251–258. http://dx.doi.org/10.1042/BJ20131412

He, T.C., A.B. Sparks, C. Rago, H. Hermeking, L. Zawel, L.T. da Costa, P.J. Morin, B. Vogelstein, and K.W. Kinzler. 1998. Identification of *c-MYC* as a target of the APC pathway. *Science.* 281:1509–1512. http://dx.doi.org/10.1126/science.281.5382.1509

He, X.C., T. Yin, J.C. Grindley, Q. Tian, T. Sato, W.A. Tao, R. Dirisina, K.S. Porter-Westpfahl, M. Hembree, T. Johnson, et al. 2007. PTEN-deficient intestinal stem cells initiate intestinal polyposis. *Nat. Genet.* 39:189–198. http://dx.doi.org/10.1038/ng1928

Hirai, H., H. Sootome, Y. Nakatsuru, K. Miyama, S. Taguchi, K. Tsujioka, Y. Ueno, H. Hatch, P.K. Majumder, B.-S. Pan, and H. Kotani. 2010. MK-2206, an allosteric Akt inhibitor, enhances antitumor efficacy by standard chemotherapeutic agents or molecular targeted drugs *in vitro* and *in vivo*. *Mol. Cancer Ther.* 9:1956–1967. http://dx.doi.org/10.1158/1535-7163.MCT-09-1012

Huang, D.W., B.T. Sherman, and R.A. Lempicki. 2009. Systematic and integrative analysis of large gene lists using DAVID bioinformatics resources. *Nat. Protoc.* 4:44–57. http://dx.doi.org/10.1038/nprot.2008.211

Jacinto, E., V. Facchinetti, D. Liu, N. Soto, S. Wei, S.Y. Jung, Q. Huang, J. Qin, and B. Su. 2006. SIN1/MIP1 maintains rictor-mTOR complex integrity and regulates Akt phosphorylation and substrate specificity. *Cell.* 127:125–137. http://dx.doi.org/10.1016/j.cell.2006.08.033

Jürchott, K., R.-J. Kuban, T. Krech, N. Blüthgen, U. Stein, W. Walther, C. Friese, S.M. Kiełbasa, U. Ungethüm, P. Lund, et al. 2010. Identification of Y-box binding protein 1 as a core regulator of MEK/ERK pathway-dependent gene signatures in colorectal cancer cells. *PLoS Genet.* 6:e1001231. http://dx.doi.org/10.1371/journal.pgen.1001231

Leystra, A.A., D.A. Deming, C.D. Zahm, M. Farhoud, T.J.P. Olson, J.N. Hadac, L.A. Nettekoven, D.M. Albrecht, L. Clipson, R. Sullivan, et al. 2012. Mice expressing activated PI3K rapidly develop advanced colon cancer. *Cancer Res.* 72:2931–2936. http://dx.doi.org/10.1158/0008-5472.CAN-11-4097

Liberzon, A., C. Birger, H. Thorvaldsdóttir, M. Ghandi, J.P. Mesirov, and P. Tamayo. 2015. The Molecular Signatures Database (MSigDB) hallmark gene set collection. *Cell Syst.* 1:417–425.

Merlos-Suárez, A., F.M. Barriga, P. Jung, M. Iglesias, M.V. Céspedes, D. Rossell, M. Sevillano, X. Hernando-Momblona, V. da Silva-Diz, P. Muñoz, et al. 2011. The intestinal stem cell signature identifies colorectal cancer stem cells and predicts disease relapse. *Cell Stem Cell.* 8:511–524. http://dx.doi.org/10.1016/j.stem.2011.02.020

Parsons, D.W., T.-L. Wang, Y. Samuels, A. Bardelli, J.M. Cummins, L. DeLong, N. Silliman, J. Ptak, S. Szabo, J.K.V. Willson, et al. 2005. Colorectal cancer: Mutations in a signalling pathway. *Nature.* 436:792. http://dx.doi.org/10.1038/436792a

Ring, D.B., K.W. Johnson, E.J. Henriksen, J.M. Nuss, D. Goff, T.R. Kinnick, S.T. Ma, J.W. Reeder, I. Samuels, T. Slabiak, et al. 2003. Selective glycogen synthase kinase 3 inhibitors potentiate insulin activation of glucose transport and utilization in vitro and in vivo. *Diabetes.* 52:588–595. http://dx.doi.org/10.2337/diabetes.52.3.588

Rommel, C., B.A. Clarke, S. Zimmermann, L. Nuñez, R. Rossman, K. Reid, K. Moelling, G.D. Yancopoulos, and D.J. Glass. 1999. Differentiation

stage-specific inhibition of the Raf-MEK-ERK pathway by Akt. *Science.* 286:1738–1741. http://dx.doi.org/10.1126/science.286.5445.1738

Samuels, Y., L.A. Diaz, O. Schmidt-Kittler, J.M. Cummins, L. DeLong, I. Cheong, C. Rago, D.L. Huso, C. Lengauer, K.W. Kinzler, et al. 2005. Mutant PIK3CA promotes cell growth and invasion of human cancer cells. *Cancer Cell.* 7:561–573. http://dx.doi.org/10.1016/j.ccr.2005.05.014

Sato, T., R.G. Vries, H.J. Snippert, M. van de Wetering, N. Barker, D.E. Stange, J.H. van Es, A. Abo, P. Kujala, P.J. Peters, and H. Clevers. 2009. Single Lgr5 stem cells build crypt–villus structures *in vitro* without a mesenchymal niche. *Nature.* 459:262–265. http://dx.doi.org/10.1038/nature07935

Sato, T., D.E. Stange, M. Ferrante, R.G.J. Vries, J.H. van Es, S. van den Brink, W.J. Van Houdt, A. Pronk, J. Van Gorp, P.D. Siersema, and H. Clevers. 2011b. Long-term expansion of epithelial organoids from human colon, adenoma, adenocarcinoma, and Barrett's epithelium. *Gastroenterology.* 141:1762–1772. http://dx.doi.org/10.1053/j.gastro.2011.07.050

Sato, T., J.H. van Es, H.J. Snippert, D.E. Stange, R.G. Vries, M. van den Born, N. Barker, N.F. Shroyer, M. van de Wetering, and H. Clevers. 2011a. Paneth cells constitute the niche for Lgr5 stem cells in intestinal crypts. *Nature.* 469:415–418. http://dx.doi.org/10.1038/nature09637

She, Q.-B., E. Halilovic, Q. Ye, W. Zhen, S. Shirasawa, T. Sasazuki, D.B. Solit, and N. Rosen. 2010. 4E-BP1 is a key effector of the oncogenic activation of the AKT and ERK signaling pathways that integrates their function in tumors. *Cancer Cell.* 18:39–51. http://dx.doi.org/10.1016/j.ccr.2010.05.023

Song, M.S., L. Salmena, and P.P. Pandolfi. 2012. The functions and regulation of the PTEN tumour suppressor. *Nat. Rev. Mol. Cell Biol.* 13:283–296. http://dx.doi.org/10.1038/nrm3330

Subramanian, A., P. Tamayo, V.K. Mootha, S. Mukherjee, B.L. Ebert, M.A. Gillette, A. Paulovich, S.L. Pomeroy, T.R. Golub, E.S. Lander, and J.P. Mesirov. 2005. Gene set enrichment analysis: A knowledge-based approach for interpreting genome-wide expression profiles. *Proc. Natl. Acad. Sci. USA.* 102:15545–15550. http://dx.doi.org/10.1073/pnas.0506580102

The Cancer Genome Atlas Network. 2012. Comprehensive molecular characterization of human colon and rectal cancer. *Nature.* 487:330–337. http://dx.doi.org/10.1038/nature11252

Thoreen, C.C., and D.M. Sabatini. 2009. Rapamycin inhibits mTORC1, but not completely. *Autophagy.* 5:725–726. http://dx.doi.org/10.4161/auto.5.5.8504

Tibshirani, R. 1996. Regression shrinkage and selection via the lasso. *J. R. Stat. Soc. B.* 58:267–288.

Tzivion, G., and N. Hay. 2011. PI3K-AKT-FoxO axis in cancer and aging. *Biochim. Biophys. Acta.* 1813:1925. http://dx.doi.org/10.1016/j.bbamcr.2011.08.014

Vidigal, J.A., M. Morkel, L. Wittler, A. Brouwer-Lehmitz, P. Grote, K. Macura, and B.G. Herrmann. 2010. An inducible RNA interference system for the functional dissection of mouse embryogenesis. *Nucleic Acids Res.* 38:e122. http://dx.doi.org/10.1093/nar/gkq199

Xue, G., and B.A. Hemmings. 2013. PKB/Akt-dependent regulation of cell motility. *J. Natl. Cancer Inst.* 105:393–404. http://dx.doi.org/10.1093/jnci/djs648

Yeh, T.C., V. Marsh, B.A. Bernat, J. Ballard, H. Colwell, R.J. Evans, J. Parry, D. Smith, B.J. Brandhuber, S. Gross, et al. 2007. Biological characterization of ARRY-142886 (AZD6244), a potent, highly selective mitogen-activated protein kinase kinase 1/2 inhibitor. *Clin. Cancer Res.* 13:1576–1583. http://dx.doi.org/10.1158/1078-0432.CCR-06-1150

Zimmermann, S., and K. Moelling. 1999. Phosphorylation and regulation of Raf by Akt (protein kinase B). *Science.* 286:1741–1744. http://dx.doi.org/10.1126/science.286.5445.1741